Ann. Geophysicae 18, 263–276 (2000) © EGS – Springer-Verlag 2000

Annales Geophysicae

Cross-field gradients: general concept, importance of multi-spacecraft measurements and study at 1 AU of the source intensity gradient for E > 30 keV solar event electrons

P. A. Chaizy[1,2]

[1] Rutherford Appleton Laboratory, Chilton, DIDCOT, Oxfordshire, OX11 0QX, Great Britain
[2] CESR, 9 Avenue du Colonel Roche, BP 4346, 31028 Toulouse Cedex 4, France

Received: 5 January 1999 / Revised: 3 August 1999 / Accepted: 26 August 1999

Abstract. Three main physical processes (and associated properties) are currently used to describe the flux and anisotropy time profiles of solar energetic particle events, called SEP profiles. They are (1) the particle scattering (due to magnetic waves), (2) the particle focusing (due to the decrease of the amplitude of the interplanetary magnetic field (IMF) with the radial distance to the Sun) and (3) the finite injection profile at the source. If their features change from one field line to another, i.e. if there is a cross IMF gradient (CFG), then the shape of the SEP profiles will depend, at onset time, on the relative position of the spacecraft to the IMF and might vary significantly on small distance scale (e.g. 10^6 km). One type of CFG is studied here. It is called intensity CFG and considers variations, at the solar surface, only of the intensity of the event. It is shown here that drops of about two orders of magnitude over distances of $\sim 10^4$ km at the Sun (1° of angular distance) can influence dramatically the SEP profiles at 1 AU. This CFG can lead to either an under or overestimation of both the parallel mean free path and of the injection parameters by factor up to, at least, ~2–3 and 18, respectively. Multi-spacecraft analysis can be used to identify CFG. Three basic requirements are proposed to identify, from the observation, the type of the CFG being measured.

Key words: Solar physics, astrophysics, and astronomy (energetic particles; flares and mass ejections) – Space plasma physics (transport processes)

1 Introduction

1.1 Description of SEP (protons and electrons)

Particles are regularly accelerated by the solar activity through magnetic recombination and/or shocks (e.g. Lin, 1974; Lin *et al.*, 1995). They are called solar energetic particle events or SEP for short. They can be accelerated in the interplanetary medium or at the Sun. Recently, comprehensive models have been proposed to describe the properties of energetic protons, of a few tens of keV to hundreds of MeV, accelerated by propagating interplanetary shocks; (e.g. Kallenrode and Wibberenz, 1997; or Lario *et al.*, 1998). Such models do not yet exist for particles accelerated at the Sun because the acceleration mechanisms are far more complex and less understood than in interplanetary shocks. Energetic particles, accelerated at the solar surfaces, present the following features: (1) a short injection at the Sun (i.e. from a few minutes to hours), (2) a fast propagation, ~30 min/AU for 30 keV electrons and (3) a total energy small enough so that they do not disturb the general pattern of the interplanetary magnetic field (IMF) (Roelof, 1969). They have been used over the last decades as tracers to get snapshots of the heliospheric conditions. For instance, they helped to understand the topology of magnetic structures (Anderson and Dougherty 1986; Lin and Kahler, 1992; Anderson *et al.*, 1992, 1995), or to identify and quantify various physical phenomena taking place in the heliosphere. Transport conditions have been studied for the last 40 years. They refer to processes influencing the particle distribution function, after the particles have left their acceleration region.

1.2 Main physical processes responsible for the observations

The observations considered in this analysis are the flux and the anisotropy time profiles of energetic (E > 30 keV) electrons accelerated at the Sun. So far, three independent physical processes have been identified to describe them. The first two are concerned with the transport condition. They are the scattering (e.g. Axford, 1965) and the focusing (Roelof, 1969) processes. The third one refers to the injection (acceleration and release) of the particles in the interplanetary medium (Reid, 1964; Axford, 1965; Schulze *et al.*, 1977). All

three processes are described together with some of the properties that had been considered and compared to observations so far.

1.2.1 Scattering. Some scattering mechanisms combined with impulsive injections at the Sun were quickly suggested to account for the properties of the intensity versus time profiles (Axford, 1965; Parker, 1965). It is now part of all models and characterised by the pitch angle diffusion coefficients, $\kappa(z,\mu)$ and/or the spatial diffusion coefficient D; note that D can be calculated from $\kappa(z,\mu)$ (e.g. Jokipii, 1966; Kunow *et al.*, 1991). Because it was shown early on that the scattering perpendicular to the IMF was negligible (e.g. Palmer, 1982) D is now understood as $D_{\|}$. The expression of $\kappa(z,\mu)$ varying from one model to another, a more convenient scalar parameter, the mean free path (λ), has been defined. The numerical value of λ can be either adjusted to the observation or calculated a priori from IMF fluctuations. Because the solar wind is a collisionless plasma (due to the low value of the proton density), a magnetic origin of the scattering is assumed when λ is calculated (Roelof, 1969). The most widely studied model has been initiated by Jokipii (1966) and Hasselmann and Wibberenz (1968); for a tutorial review see Kunow *et al.* (1991). The model considers the non-adiabatic resonant interaction of small magnetic irregularities, which is also called the quasi-linear theory (QLT). The magnetic field irregularities, input in the QLT, are generally waves described by the power spectral tensor. The "slab model", used in combination with the QLT, considers that the waves are Alfvèn waves. The comparison between theory and observations frequently, but not always (e.g. Wanner and Wibberenz, 1993), shows qualitative and quantitative discrepancies (e.g. Wibberenz *et al.*, 1970; Palmer, 1982; Kallenrode, 1993). For instance, for MeV protons, theoretical values of the parallel mean free path are usually smaller than their observational counterparts by a factor $\sim$10. This implies that the observations and/or the theory are either wrong or incomplete. The identification of mechanisms, other than scattering, acting on the shape of those SEP flux and anisotropy profiles, hereafter called SEP profiles, is therefore fundamental to make a good description of the diffusion coefficient. Those mechanisms could be either some independent physical processes, such as the injection profile or the focusing, or properties of the scattering. The latter have attracted a lot of the attention. Some examples of what have been studied so far are given. However, because it would be too long to develop and because some questions are still open the conclusions are not reviewed. Instead, examples of references, among the most recent ones addressing the subject, are provided.

1. Does the mean free path have a radial dependency (λ deduced from the time profiles observation is actually an average value along **B**.)? (e.g. Kallenrode, 1993; Wanner and Wibberenz, 1993).
2. How are the electron and proton mean free paths related? (e.g. Kallenrode, 1993; Bieber *et al.*, 1994).
3. Does diffusion coefficient depend on the rigidity (R)? (e.g. Palmer, 1982; Kunow *et al.*, 1991; Kallenrode, 1993; Bieber *et al.*, 1994) where $R = \frac{Pc}{z\lvert e\rvert}$ where P is the particle momentum, c the velocity of light, z the atomic number and e the electronic charge.
4. Can a scattering across magnetic field lines influence the time profile significantly? (Morfill *et al.*, 1979; Scholer *et al.*, 1979; Wanner and Wibberenz, 1993).

1.2.2 Focused transport. The main idea of the focused transport process is to collimate the particles along the field line via the divergence of the IMF, i.e. via the tendency to conserve the first adiabatic invariant. A differential equation combining both the scattering and the focused transport has been proposed by Roelof (1969). It assumes that the energy of the particles does not change. This implies that the particles that can be described by this equation must move fast enough so that the influence of the solar wind convection and of the adiabatic deceleration (due to the expansion of the plasma in the interplanetary medium) can be considered as negligible. In Roelof's (1969) equation, the focusing is characterised by the variation of a static magnetic field with the radial distance to the Sun: **B**(r). Therefore, the expression of **B**(r) can influence the SEP profiles. Ng and Wong (1979) performed the study assuming a monopolar, archimedean or exponential magnetic field. Unlike the scattering or finite injection profile, no observational features have been proposed to separate the respective influence of **B**(r) and of the diffusion coefficient. This means that to find one we have to assume the other. In the models, it is usually **B**(r) that is assumed and described by an archimedean spiral of which main parameter is the average solar wind speed at the time of the event.

1.2.3 Finite injection profile. Reid (1964) and Axford (1965) proposed a scenario in which the flux and anisotropy profiles resulted from the combination of a finite injection (as opposed to a time delta-function injection) followed by some scattering mechanism. However, it was not until 1977 that Schulze *et al.* proposed to quantitatively estimating the relative influences on the anisotropy of the scattering and of the finite injection profile.

Numerous models have been proposed to study the injection of the particles from the solar corona into the interplanetary medium (see Kunow *et al.*, 1991 for review). All those models use parameters, like t_c and t_l in Eq. (5), of which numerical values is obtained by fitting indirect measurements, like the flux and the anisotropy at 1 AU. Unfortunately, so far, there were no direct observations of injection profiles thus preventing an exact checking of the quality of the numerical values got and, subsequently, of the models. However, the high quality of the new ISTP (International Solar

Terrestrial Physics) data is currently bringing new insight in that matter (e.g. Maia *et al.*, 1998; Pick *et al.*, 1998).

1.3 Interest of this paper

Because of the convection, which reduces to corotation in a steady state, of the IMF, if one or several parameters describing the SEP profiles vary from one field line to another then the measured profiles will be highly dependent on the position of the spacecraft. In this work this phenomenon has been given the generic name of cross-field gradients or CFG for shorter. This concept is not new (e.g. Ng and Gleeson, 1976) and is usually presented in the context of a case study. For instance, coronal transport can certainly create CFG by changing the amplitude and shape of the injection profile from one field line to another. From this assumption, Wiberrenz *et al.* (1989) showed that they could reproduce the observations of two events made by Helios 1 and 2 and by Prognoz 6. However, earlier, Morfill *et al.* (1979) showed that, at 1 AU, assuming a magnetic (QLT) origin of the scattering, the diffusion coefficient could vary with the solar longitude. Following that observation, Scholer *et al.* (1979) showed that this scattering across IMF lines could also have significant impacts on the SEP profiles. This leads to questions like: (1) *from the observation point of view, how can we separate CFG due to coronal transport from CFG due to variable scattering conditions?* or (2) *Can CFG be generated by other mechanisms than the two described?*

Using as support the case study of variation of the intensity of the injection at the source, called hereafter intensity CFG, this work addresses the following questions:

1. What are the features of the intensity CFG?
2. What can be the consequences of neglecting the CFG when estimating the classic parameters? For simplicity let us call *classic parameters* the mean free path parallel to **B** and the injection profile parameters (λ, t_c and t_1, see later), the *CFG parameters* the parameters controlling the shape of the gradient (a, b, c and d, see later) and the *searched parameters* the classic plus CFG parameters.
3. How can several spacecraft be used to detect and identify the origins of CFGs from observations?

2 The intensity CFG

In this chapter, the general concept of CFG and its influence on the SEP profiles is first presented. Then, the particular case of intensity CFG and the model used to implement it, are described. Finally, a quantitative analysis of the influence of the intensity CFG on the SEP profiles and, more particularly, on the classic parameters values is given.

2.1 The concept of CFG

Electron flux time profiles measured at two closely located spacecraft should be similar if, during all the duration of the event, the convected magnetic field lines crossing the spacecraft, are always connected to the same acceleration/release/propagation region. In the case of CFG, both spacecraft are crossed by the same field lines but the latter are not connected to the same acceleration/release/propagation region. This is illustrated on Fig. 1. This lack of homogeneity creates flux profiles that vary, in the solar wind frame, from one field line to another. Due to the solar wind convection, the spacecraft moves across those field lines. Therefore, the profile that it will measure will be a space-time cut of the time intensity profiles on each field line and of its trajectory across them. Because the relevant part of the trajectory starts at the onset time two spacecraft positioned differently, along an identical solar wind path, will have two distinct trajectories through the IMF. Hence, the shape of the measured time profiles will vary with respect to the position of the spacecraft, at onset time.

It has to be noted that, in Fig. 1, it is assumed that both spacecraft record the onset at the same time, i.e. that they are located at the same distance from the source. This assumption is valid for the near-Earth ISTP spacecraft. Indeed, the maximum radial distance that separates Earth orbiting spacecraft from spacecraft situated at the Lagrangian point or on elongated orbit, like WIND, ACE or SOHO, is of the order of 10^6 km. Such separation at 1 AU has little impact on the distance to the Sun along the spiral field line

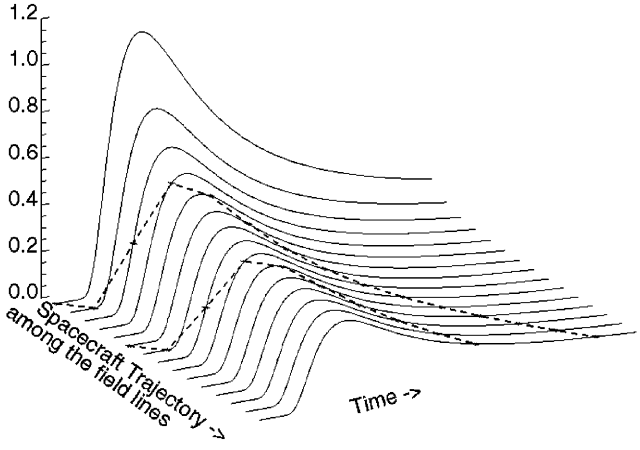

Fig. 1. This describes the CFG concept. Each *solid line* represents flux profiles that could be measured, in the solar wind frame, on individual adjacent field lines. Intensity CFG has been chosen as example; i.e. the maximum varies from one field line to another. Because of the convection, spacecraft will go through those field lines as time goes on. Therefore, the profile measured at the spacecraft will be the convolution of the flux profiles on each field line with its trajectory among the latter. It will vary with the position of the spacecraft, along the solar wind path, at the onset time. The *dashed line* represents profiles that would be measured by two spacecraft located at different radial distance from the Sun, at the injection time, with such CFG

(~1%). However, it is very significant for the convection since it will take typically ~1 h for a field line seen at the Lagrangian point to reach an Earth orbiting spacecraft.

2.2 The model for the intensity CFG

To get the profiles at one spacecraft one has first to provide time profiles on each field lines and calculate the convoluted profile for a given trajectory, i.e. spacecraft position.

2.2.1 SEP profiles with delta-function injection on individual IMF lines. Initial SEP profiles are generated using a model considering all three main physical processes and detailed by, e.g., Kallenrode (1993). The transport, scattering and focusing processes, are described by Roelof's (1969) equation which provides, when integrated, the distribution function $f(z,\mu,t)$:

$$\frac{\partial f}{\partial t}+\mu v\frac{\partial f}{\partial z}=-\frac{1-\mu^2}{2L}v\frac{\partial f}{\partial \mu}+\frac{\partial}{\partial \mu}\left(\kappa(z,\mu)\frac{\partial f}{\partial \mu}\right) \tag{1}$$

where z is the distance travelled by the particles along **B**, μ is the cosine of the pitch angle, v the particle velocity, $\kappa(z,\mu)$ the pitch angle diffusion coefficient and L the focusing length given by the expression (first adiabatic invariant):

$$L=-B(z)\Big/\frac{\partial z}{\partial B} \tag{2}$$

This above equation provides a delta function injection at the Sun, f, i.e. an injection of all particles in a time infinitely short. However, the real injection time takes a while. Therefore, finite injection profiles are required to describe the profiles seen by the spacecraft. For collisionless plasma, they influence the profiles at a given spacecraft according to the following relation (Schulze *et al.*, 1977):

$$F(t,z,\mu)=\int_0^t I(\tau)\times f(t-\tau,z,\mu)\mathrm{d}\tau \tag{3}$$

where F represents the flux time profile at the distance z from the source, at the time t, and pitch angle cosine μ. $I(\tau)$ is the intensity time profile of the source at the Sun.

The model and its limitations have already been described many times in the literature (e.g. Kunow *et al.*, 1991; Kallenrode, 1993) and, therefore, will not be re-described again here. Rather, the key inputs to the model used here are provided i.e.:

1. Consistently with previous work (e.g. Kallenrode, 1993), λ_r, the radial mean free path is kept constant. λ_r is related to the parallel (to **B**) mean free path, $\lambda_\parallel$, by the relation:
$$\lambda_r=\lambda_\parallel\cos^2\psi \tag{4}$$
where ψ is the angle between the Sun-spacecraft line and the archimedean magnetic field.
2. The solar wind speed required to calculate L has been arbitrarily taken as to 440 km/s.
3. The analytical form of the initial z and μ distribution is given by Ng and Wong (1979). The parameters have been chosen so that the spatial distribution: (a) is narrow along z: the FWHM of the distribution has been arbitrarily taken equal to about 0.015 AU; (b) is close to the Sun: the distance to the Sun of the maximum of the distribution function is about 0.024 AU; and (c) the initial function is quasi-isotropic.
4. The intensity time profile of the source at the Sun used is the Reid-Axford profile:
$$I(t)\propto\frac{1}{t}\exp\left(-\frac{t_c}{t}-\frac{t}{t_l}\right) \tag{5}$$
where t_c is the coronal diffusion and t_l the loss time (Kunow *et al.*, 1991).
5. The numerical value of $\lambda_\parallel$ is derived from the pitch angle diffusion coefficient by the expression (Jokipii 1966; Hasselmann and Wibberenz, 1968) for diffusive model:
$$\lambda_\parallel=\frac{3v}{8}\int_{-1}^{+1}\frac{(1-\mu^2)^2}{\kappa(\mu)}\mathrm{d}\mu \tag{6}$$
This relation has been established assuming a purely diffusive transport mechanism. This means that for weak scattering, the focusing process is going to become predominant and will modify the meaning of that expression. However, as pointed out many times (e.g. Wanner and Wibberenz, 1993) it can still give an idea of the scattering strength of the interplanetary medium.

2.2.2 Implementation of the intensity CFG in the model. Heliolongitude variations of the intensity of the injection profile can be described by radial variations for a given time and Sun-spacecraft direction. The corotation can then be described by the convection of that radial profile along the same Sun-spacecraft direction. This means that both spacecraft are crossed by the same field lines, propagating radially from the Sun with a constant ψ angle, and carrying each a distinct intensity value of the injection profile. This scenario is mathematically described by the coefficient $\mathrm{A}(r)$ added to the Reid-Axford equation, r being the radial distance to the Sun:

$$I(t)=\mathrm{A}(r)\frac{1}{t}\exp\left(-\frac{t_c}{t}-\frac{t}{t_l}\right) \tag{7}$$

Within that scenario, the numerical expression of $\mathrm{A}(r)$ has been arbitrarily chosen as equal to:

$$\mathrm{A}(r)=\begin{cases}a\times\exp\left(\frac{-(r-b)^2}{c}\right)+d & 0\le r\le b\\ a+d & b\le r\end{cases} \tag{8}$$

This equation provides a wide range of density profiles of which values evolve between $a + d$ and d.

2.2.3 Influences of the numerical integration on the time profile. One of the effects of the numerical integration becomes less and less negligible when the focusing and the scattering are weak simultaneously, i.e. when the particles are far from the Sun and when the mean free path is large. When such a situation occurs, the particles do not move from one pitch angle to another. Particles with low pitch angles will propagate faster than particles with high pitch angle and will be separated from the latter. In extreme conditions, i.e. far away from the Sun with no focusing and no scattering, the flux would be a succession of discrete arrivals of particles. Within the conditions encountered in this work, and more particularly with a λ_r of 1.1 AU, the effects of the numerical integration are present but limited. For instance, there are "bumps" in the decay phase of the SEP profiles. Because these effects increase with λ_r, profiles with high mean free path must be considered cautiously. To reduce that effect, one could decrease the step values used in the integration. However, it would increase the integration time, already quite long on the computer used.

2.3 The analysis: method and results

The aim of this analysis is to assess the influence of the intensity CFG on the SEP profiles and on the determination of the classic parameters. Before giving the results, it is first shown how the χ^2 has been used for both objectives.

2.3.1 Use of the χ^2. The χ^2 quantity is very appropriate to assess how different or, equivalently, similar, are two profiles. It is therefore very suitable to achieving both objectives. The χ^2 is defined by the expression (e.g. Bevington and Robinson 1994):

$$\chi^2 \equiv \sum_{n=1}^{N} \frac{(y_n^a - y_n^b)^2}{(\sigma_n^a)^2 + (\sigma_n^b)^2} \tag{9}$$

where y^m is a population of N data points (measured or theoretical) and σ_n^m the standard deviations of each data point of each population; here, each y_n value is considered being an average value with an uncertainty. If the analytical function is correct, N large enough, and the values of σ_n^m well estimated then, in average:

$$(y_n^a - y_n^b)^2 = \frac{(\sigma_n^a + \sigma_n^b)^2 + (\sigma_n^a - \sigma_n^b)^2}{2} \tag{10}$$

$$(y_n^a - y_n^b)^2 = (\sigma_n^a)^2 + (\sigma_n^b)^2 \tag{11}$$

in other words:

$$\chi^2 \approx N \tag{12}$$

In reality, the expression used is the reduced chi-square that must be close to one:

$$\chi_v^2 \equiv \frac{\chi^2}{v} \tag{13}$$

where v is the total number of degrees of freedom.

To study the relative influence of the searched parameters on the flux and anisotropy profiles, v is equal to N, the total number of data points. To assess the impact of the CFG on the values of the classic parameters, at a given location of the heliosphere, flux and anisotropy profiles first have to be created using the CFG. Then the values of the classic parameters have to be fitted without any CFG. Once done we can assess the influence of the CFG by comparing the "true" to the "apparent" values. This requires the simultaneous fitting of several independent profiles which is accessible to the χ^2 method. Indeed, fitting data using the chi-square method aims to minimise the quantity:

$$\chi^2 \equiv \sum_{n=1}^{N} \left(\frac{y_n - y(x_n; a_1 \cdots a_M)}{\sigma_n} \right)^2 \tag{14}$$

What has to be noted is that σ_n is associated with each data point individually (see later for a definition of σ_n). This means that the expression would still be valid even if two functions were fitted simultaneously under the same χ^2:

$$\chi^2 \equiv \sum_{n=1}^{N} \left(\frac{y_n - y(x_n; a_1 \cdots a_l)}{\sigma_n} \right) + \sum_{m=1}^{M} \left(\frac{y_m - y(x_m; b_1 \cdots b_p)}{\sigma_m} \right)^2 \approx N + M \tag{15}$$

In that case, v, the degree of freedom used in the calculation of the χ_v^2 equals: $N + M - P$, where $N + M$ represents the total number of data points, all profiles included and P the number of parameters. The Marquardt-Levenberg (see Bevington and Robinson, 1994; Numerical Recipes, 1989) method has been used to fit the data.

It is clear, from this mathematical expression of the χ_v^2, that the estimation of the σ_n^t, where n is the spacecraft id and t the type of profile, is going to be of major importance in determining the χ_v^2 values. Following the justifications provided in the Appendix, the expressions presented hereafter have been used, for the flux and anisotropy uncertainties (i.e. σ_n^f and σ_n^a, respectively).

Flux uncertainty:

$$\sigma^f = \alpha^f \sqrt{y^f} \tag{16}$$

Anisotropy uncertainty:

$$\sigma^a = \frac{\alpha^a}{\sqrt{y^a}} \tag{17}$$

Where y_n^f represent the flux values, α^f and α^a two arbitrary coefficients. For simplicity, it has been assumed that those values are the same on both spacecraft

so justifying the drop of the n index. The meaning of χ^2_υ value will therefore depend on the meaning of the α^f and α^a coefficients. To compare one simulated profile, or fit, to another, the α^f and α^a coefficients have been assumed known and, therefore, kept identical.

2.3.2 Searched parameters and position of the spacecraft. The number of combinations of the key parameters (e.g. solar wind speed, spacecraft positions, injection profile, diffusion coefficient...) is, of course, very large. Therefore only a few scenarii are presented and developed here as examples. The range of values used is presented in Table 1. A spacecraft configuration similar to the one of the ISTP spacecraft has been used. The intensity CFG features, accessible to such configuration, have been studied.

It has already been shown (Schulze *et al.*, 1977) that the anisotropy and flux profiles respond differently to the injection profile. Therefore, in order to simplify the analysis, only comparisons of profiles of the same type have been done (i.e. flux versus flux and anisotropy versus anisotropy).

Looking at Figs. 2 and 3, what stands out is the influence of the sharpness of the intensity CFG on the profiles. One can see that sharp decreases have almost no effect (Fig. 2a) while moderate decreases influence the region of flux profile situated around two hours after onset (Figs. 2b, c and 3). Long decreases influence mostly the decay phase of the flux profiles (Fig. 2d).

Table 1. Range of parameter values used during the simulations of the flux and anisotropy profiles

Radial distance to the Sun of both spacecraft: ~1 AU from the Sun (i.e. ~1.2 AU along Parker's spiral with a solar wind speed of ~440 km/s)
Convection time in between the 2 spacecraft: 45 min, which corresponds to a radial distance of $\sim 1.2 \times 10^6$ km with a convection speed of ~440 km/s
Energy of the particles: ~26 keV
Background level before onset: 10 part./cm^2. s.sr.keV
Maximum flux without background: 1000 part./cm^2. s.sr.keV
Flux and anisotropy uncertainty coefficients: $\alpha^f = 1.0$ and $\alpha^a = 0.3$
Mean free path, λ_r, in AU: 0.08 AU, 0.27 AU and 1.11 AU (for SEP profiles comparison only), typical values of the Palmer consensus
Parameters of Eq. (11) controlling the amplitude of the intensity CFG: • $a = 5 \times 10^{-4}$, $d = 500$; i.e. the intensity of the density at the source will decrease by ~2 orders of magnitude • $b = 1.0$ AU; i.e. the intensity starts decreasing at the field line connecting the downstream spacecraft at the time of the injection • $c = 10^{-5}$, 10^{-4} and 10^{-3}, i.e. such that the intensity CFG is high, intermediate and low • the gradient has a positive slope in direction pointing outward from the Sun
Let's call positive intensity CFG, intensity CFGs for which the intensity increases from east to west at the Sun; i.e. the chosen case for the analysis
Parameters controlling the shape of the Reid-Axford injection profile: $(t_c, t_l) = (1.5, 0.5)$, (0.5, 0.1) and (1.5, 2.0); i.e. a fairly short, intermediate and fairly long injection profile duration

Fig. 2a–d. Provides some examples of profiles that can be obtained with the intensity CFG. It focuses on the influence of the c parameter. Figure 3 focuses on the influence of the λ_r and (t_c, t_l) parameters with the value of c that provides the maximum of discrepancy between the profiles of the two spacecraft. The *first panel* shows, at the time of injection, the source density gradient, across the field lines, projected at one AU. With time, the profile moves towards the right, with respect to the frame of the panel. The *two axes* represent the position of the spacecraft *with respect to the profile* (i.e. not to the frame) at the time of onset. This means that at the time of the beginning of the injection, the two axes are shifted right so that the axis of the downstream spacecraft coincides with one AU. The *second* and *third panels* represent respectively, the flux and anisotropy profiles. The *dotted* and *short dashed lines* represent respectively, the profile measured by the downstream and upstream spacecraft. The *long dashed line* is the profile that would be measured if there were no intensity CFG. The maximum of that latter profile is arbitrarily set to the highest maximum of the two other profiles; here 1000 part./cm^2.s.sr.keV. It has to be noted that the background level, set here at 10 part./cm^2.s.sr.keV, plays an important role in the profiles, mainly the anisotropy (it rounds, reduces and shifts the anisotropy maximum). The existence of discrepancies, between the upstream and downstream spacecraft anisotropy profiles, is only due to the background level. The α^f and α^a coefficients have been arbitrarily set to 1.0 and 0.3, respectively, in the calculation of the χ^2_υ value comparing the profiles at both spacecraft. The *fourth panel* shows the injection profile at the source

Some interesting features, like the broken rising flux profile of the upstream spacecraft of Fig. 2c, can also be seen. Probably one of the most interesting ones is that intensity CFG can create peaks in the flux profile (e.g. Fig. 2b, c) that are very similar to those usually associated to scatter-free events (e.g. Lin, 1974). The probability of misinterpretation is described in the next section.

For a quantitative estimate of the influence of the searched parameters, for a given spacecraft configuration, an analysis of the χ^2_υ values has been performed. Table 2a shows the variations of the χ^2_υ values with respect to the λ_r, t_c, t_l and c parameters, for a given spacecraft configuration. The influence of the position of the spacecraft on the SEP profile increases with the χ^2_υ value. The anisotropy χ^2_υ values always show small values. If they were coming from measurements, they would indicate no significant discrepancy between the profiles. Therefore, with the intensity CFG, anisotropy profiles are unlikely to show significant variations from one spacecraft to another. Oppositely, the flux χ^2_υ shows big variations with meanings going from insignificant to very significant discrepancies between the profiles. Therefore, hereafter, any reference to "χ^2_υ" will mean "χ^2_υ of the flux profile".

The main fact is that the χ^2_υ values depend on two factors: the duration and the amplitude of the discrepancy between the two profiles. Let us see how these parameters play on these two factors.

Variation of the χ^2_υ with c is not monotonic (Table 2a). It goes to a maximum at $c = c_{max} = 10^{-4}$ (note that the real c_{max} is not necessarily equal to 10^{-4}).

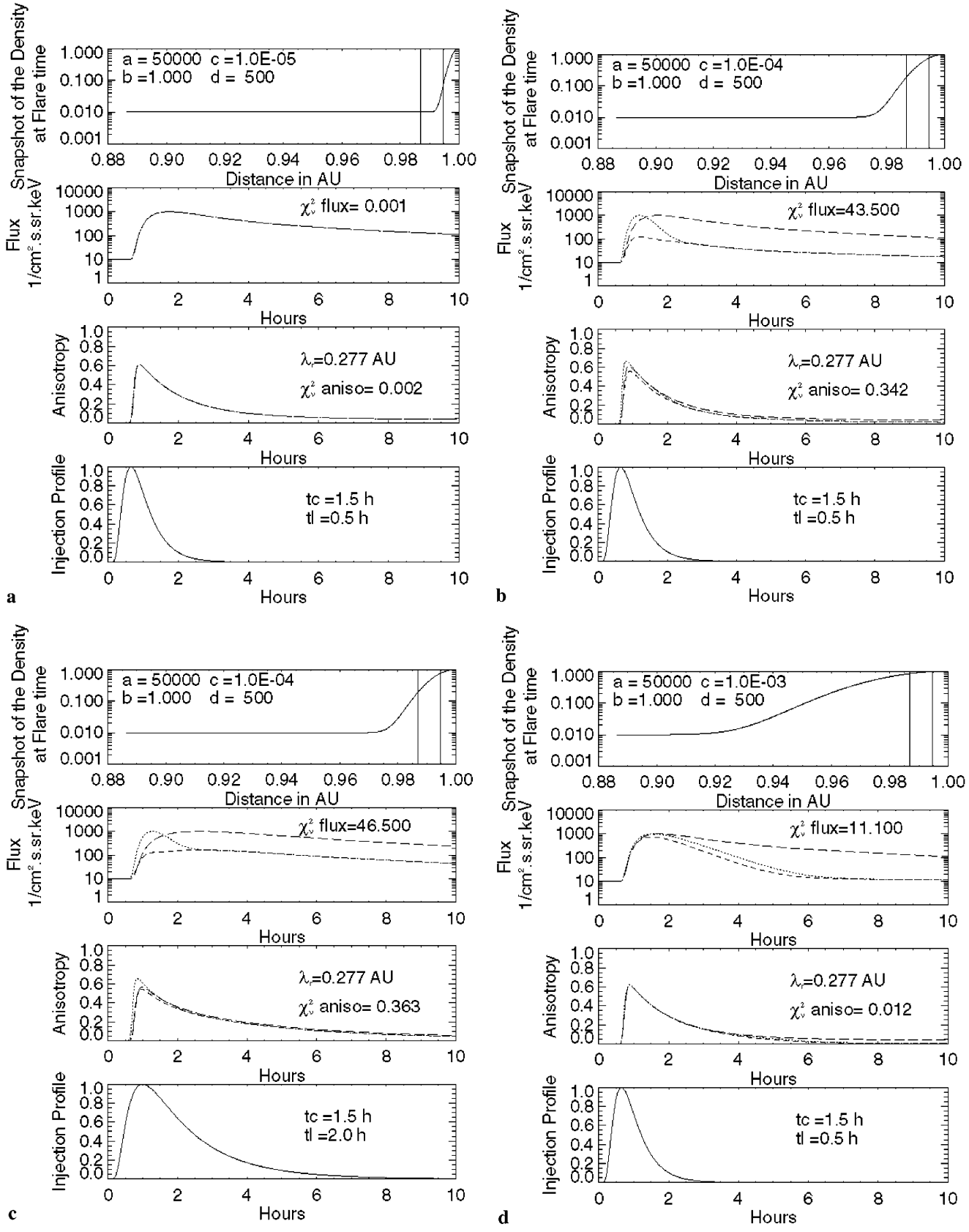

Indeed, a high gradient would make the difference at the two spacecraft big but limited to a short period, close to the onset. Oppositely, a slow gradient would make the differences extend through a long period but small. Therefore, the biggest χ^2_υ must be found for intermediate values of the amplitude of the gradient.

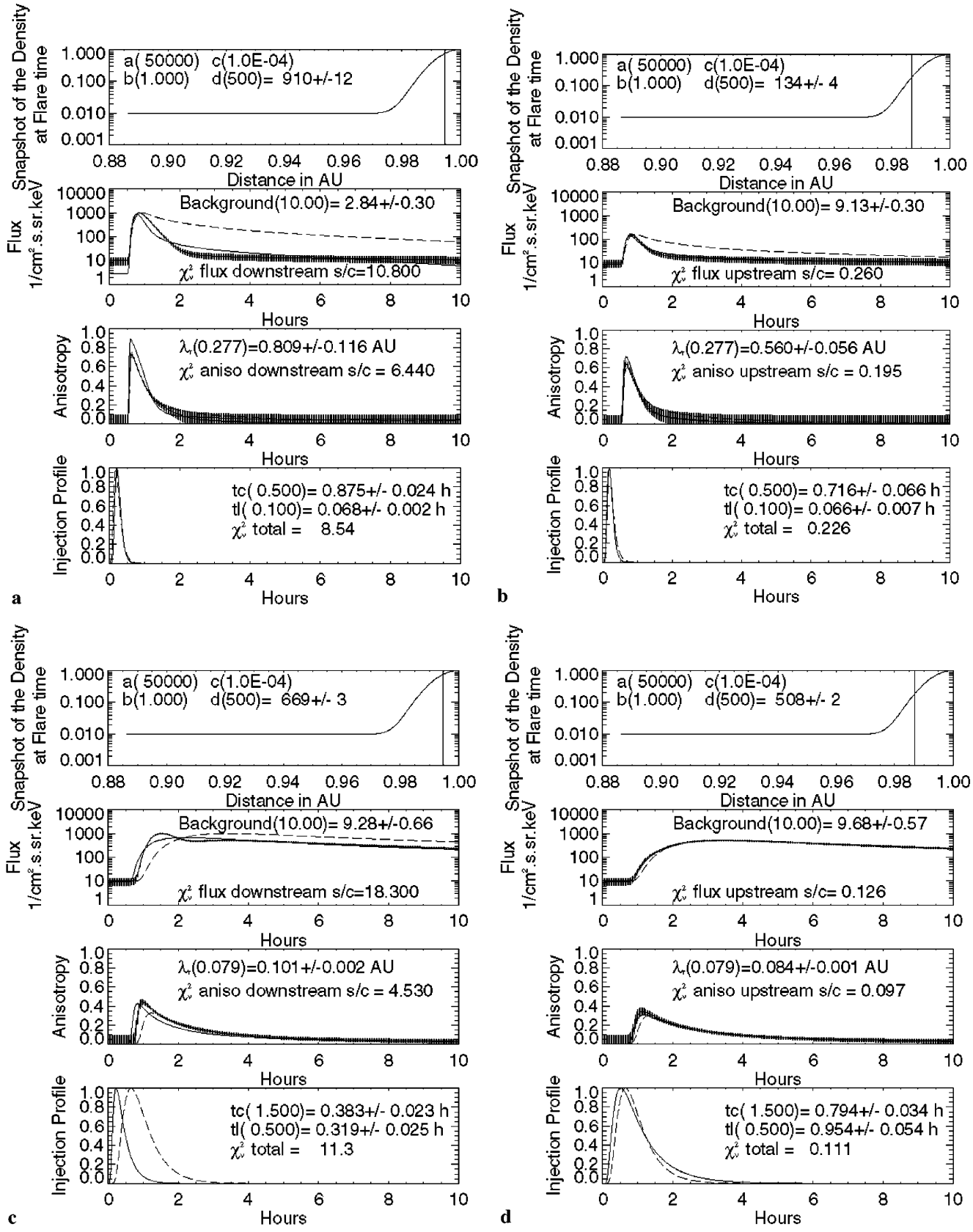

The χ_v^2 is also governed by the slope of the "true" flux profile at the time of influence of the CFG (Table 2b). For a given c value, a slow variation should reduce the amplitude of the discrepancy while a rapid one should increase it, so reducing the χ_v^2 value. However, this effect would be also balanced by a modification of the duration

Fig 3a–f. Shows the influence of the intensity CFG on the classic parameter values. *Panels* are similar to those of Fig. 2. The numerical values of the maximum flux, background level, α^f and α^a coefficients are the same as for Fig. 2. However, profiles of only one spacecraft are shown and used to simulate data with error bars. The outcome of the fit, considering no CFG, of the classic parameters is plotted with the *solid line*. The "true" numerical values are given within *parenthesis* while the outcome of the fit is given with the uncertainty. As for Fig. 2, the profile that would be measured, if there were no intensity CFG, is plotted with a *long dashed line*. This figure is also used to show complementary examples to Fig. 2. It focuses on the influence of the λ_r and (t_c, t_l) parameters, with the value of c that provides the maximum discrepancy between the profiles of both spacecraft

of the period of discrepancy: a slow variation would make the discrepancy lasting longer. This can be seen in Table 2b in which the classic parameter values are first sorted according to c then to the χ^2_v. For values of $c > \sim c_{max}$ the influence of the duration will overwhelm the influence of the amplitude of the discrepancy because the latter is mostly located in the decay phase. This is exactly the opposite for $c < \sim c_{max}$ exhibiting a discrepancy mostly located in the early phase of the event. Therefore, values of the classic parameters decreasing the absolute value of the flux profile gradient, increase and decrease the χ^2_v, respectively for values of $c > \sim c_{max}$ and $c < \sim c_{max}$. For instance, a decrease of λ_r will increase the χ^2_v for $c = 10^{-3}$ and decrease it for $c = 10^{-5}$.

Influence of other parameters can be deduced from the above analysis. For instance, for a given set of values of the classic parameters, positioning the upstream spacecraft closer to the Sun would certainly increase the χ^2_v value because of an increase in the amplitude of the discrepancy. In addition, a decrease of the d value would increase the duration of the influence of the discrepancy and, therefore, also the χ^2_v value.

Negative intensity CFG have also been examined. As expected, the flux profiles are different and inverted: the upstream spacecraft presents a higher profile than the downstream one. However, the general discussion about the influence of each individual parameter is similar.

One can also look at the scale of the variation of the intensity at the Sun. Following the expression given by Anderson and Dougherty (1986), to calculate the width of interplanetary structures, the width of the CFG region perpendicular to the IMF can be estimated by the expression:

$$W = \Delta R \sin(\psi) \tag{18}$$

where ΔR is the radial width of the structure. Once done, a gross estimation of the width at the Sun, *Ws*, can be extrapolated. At 1 AU, W also represents the swept angular distance Φ in radians which, in the ecliptic plane, is equivalent to the difference in heliolongitude. Therefore, assuming $\psi = 45°$, we have:

c	ΔR (AU)	W (AU)	*Ws* (km)	Φ in degrees
10^{-3}	~0.080	~0.057	~40 000.00	~3.2°
10^{-4}	~0.020	~0.014	~10 000.00	~0.8°
10^{-5}	~0.005	~0.004	~2500.00	~0.2°

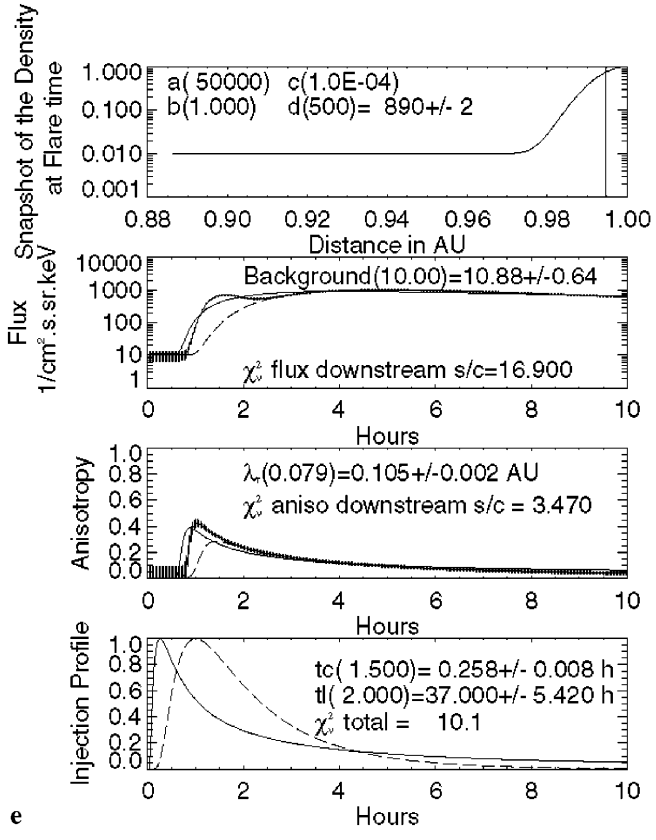

e

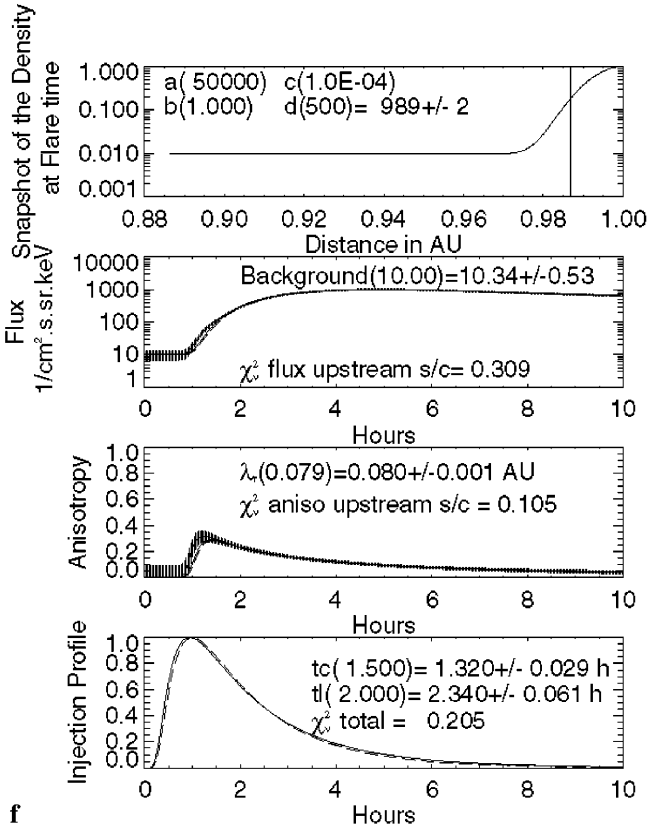

f

Fig. 3 Continued

Table 2. Variations of the importance, with respect to the λ_r t_c, tl, and c parameters, of the position of the spacecraft, within the IMF lines at onset time: the importance increases with the χ^2_υ

λ_r (AU)	t_c (h)	t_l (h)	c (AU^2)	χ^2_υ Flux	χ^2_υ Anisotropy
a					
0.08	1.5	2	1.00E−05	1.73E−08	4.99E−08
0.08	1.5	0.5	1.00E−05	2.82E−07	6.94E−07
0.28	1.5	2	1.00E−05	1.98E−04	4.44E−04
0.28	1.5	0.5	1.00E−05	1.14E−03	1.53E−03
0.08	0.5	0.1	1.00E−05	2.15E−03	1.75E−03
1.11	1.5	2	1.00E−05	7.95E−03	9.16E−03
1.11	1.5	0.5	1.00E−05	2.39E−02	1.54E−02
0.28	0.5	0.1	1.00E−05	6.43E−01	4.64E−02
1.11	0.5	0.1	1.00E−03	6.55E−01	4.22E−03
1.11	0.5	0.1	1.00E−05	2.40	7.39E−02
1.11	1.5	0.5	1.00E−03	4.16	4.53E−02
0.28	0.5	0.1	1.00E−03	4.71	6.74E−03
1.11	1.5	2	1.00E−03	10.46	2.21E−01
0.28	1.5	0.5	1.00E−03	11.14	1.16E−02
1.11	0.5	0.1	1.00E−04	16.24	3.95E−01
0.08	0.5	0.1	1.00E−03	18.21	4.64E−03
0.28	1.5	2	1.00E−03	18.83	2.35E−02
0.08	1.5	0.5	1.00E−03	23.61	6.64E−03
0.08	1.5	2	1.00E−04	28.77	2.26E−01
0.08	1.5	2	1.00E−03	29.99	8.11E−03
0.28	0.5	0.1	1.00E−04	30.66	2.23E−01
1.11	1.5	0.5	1.00E−04	37.46	7.56E−01
0.08	1.5	0.5	1.00E−04	42.09	2.03E−01
0.28	1.5	0.5	1.00E−04	43.50	3.42E−01
1.11	1.5	2	1.00E−04	43.82	6.82E−01
0.28	1.5	2	1.00E−04	46.55	3.63E−01
0.08	0.5	0.1	1.00E−04	46.64	1.54E−01
b					
0.08	1.5	2	1.00E−05	1.73E−08	4.99E−08
0.08	1.5	0.5	1.00E−05	2.82E−07	6.94E−07
0.28	1.5	2	1.00E−05	1.98E−04	4.44E−04
0.28	1.5	0.5	1.00E−05	1.14E−03	1.53E−03
0.08	0.5	0.1	1.00E−05	2.15E−03	1.75E−03
1.11	1.5	2	1.00E−05	7.95E−03	9.16E−03
1.11	1.5	0.5	1.00E−05	2.39E−02	1.54E−02
0.28	0.5	0.1	1.00E−05	6.43E−01	4.64E−02
1.11	0.5	0.1	1.00E−05	2.40	7.39E−02
1.11	0.5	0.1	1.00E−04	16.24	3.95E−01
0.08	1.5	2	1.00E−04	28.77	2.26E−01
0.28	0.5	0.1	1.00E−04	30.66	2.23E−01
1.11	1.5	0.5	1.00E−04	37.46	7.56E−01
0.08	1.5	0.5	1.00E−04	42.09	2.03E−01
0.28	1.5	0.5	1.00E−04	43.50	3.42E−01
1.11	1.5	2	1.00E−04	43.82	6.82E−01
0.28	1.5	2	1.00E−04	46.55	3.63E−01
0.08	0.5	0.1	1.00E−04	46.64	1.54E−01
1.11	0.5	0.1	1.00E−03	6.55E−01	4.22E−03
1.11	1.5	0.5	1.00E−03	4.16	4.53E−02
0.28	0.5	0.1	1.00E−03	4.71	6.74E−03
1.11	1.5	2	1.00E−03	10.46	2.21E−01
0.28	1.5	0.5	1.00E−03	11.14	1.16E−02
0.08	0.5	0.1	1.00E−03	18.21	4.64E−03
0.28	1.5	2	1.00E−03	18.83	2.35E−02
0.08	1.5	0.5	1.00E−03	23.61	6.64E−03
0.08	1.5	2	1.00E−03	29.99	8.11E−03

For Table 2a, the values are sorted according to the flux χ^2_υ only. For Table 2b they are first sorted according to c then to the flux χ^2_υ

This shows that spacecraft separated by 10^6 km at 1 AU ($\Phi \approx 0.3°$) can detect variations over spatial distances of the order of a few thousands kilometers of the Sun or, equivalently, of $\sim 1°$ in angular distances.

2.3.3 Influence of the intensity CFG on the classic parameters. One way of assessing the impact of the intensity CFG on the classic parameters, is to adjust the latter by fitting simulated flux and anisotropy CFG profiles, from one spacecraft, and assuming no CFG. Once done, one can compare the fitted and true values as well as the fitted values obtained from one spacecraft to another. Fits have been done for all the combinations of the searched parameters given in the previous section but for the $\lambda_r = 1.11$ AU due to the numerical integration effect at these low values. They have been done for both the upstream and downstream spacecraft. The influence of the intensity CFG on the classical parameters is summarised in Tables 3 and 4. Table 3 gives the rate of success for the various sets of searched parameter values. In all cases, at the beginning of the fit, the initial values of the classic parameter were the true values.

The fact that all fits converged successfully when the influence of the intensity CFG is small ($c = 10^{-5}$) is not surprising. It is also uninteresting since the obtained values are similar to the true one. The lack of success for $c = 10^{-3}$ can be due to the lack of good initial parameter values when starting the fit, of α^f and α^a not well chosen, etc. However, more likely, some of the profiles obtained with the intensity CFG cannot be described only with the classic parameters. In other words, the various combinations of mean free path value and injection profiles do not cover an infinite range of flux and anisotropy set of profiles.

The c value that gives the biggest difference of the flux profiles between the upstream and downstream spacecraft produces the fit that is most likely to succeed. In that case the failure of some of the fits are more likely due to poor initial conditions. Indeed, changing the initial conditions on some of the failing cases, leads to almost successful fits.

Table 4 gives the values of the classic parameters found for the successful, or quasi-successful, fit. Figure 3 provides a visual appreciation of the quality of the fit.

Table 3. Summary of the fit outcomes of the simulated profiles. There are three sets of (t_c, t_l) couples taken for each value of c and λ: (0.5, 0.1), (1.5, 0.5) and (1.5, 2.0). An unsuccessful fit is a fit that provided negative values and/or a big χ^2_υ. A "close to successful fit" is a fit that would be likely to provide a smaller χ^2_υ value if the error bars, i.e. α^f and α^a, were slightly bigger

	$\lambda_r = 0.277$ AU	$\lambda_r = 0.0792$ AU
Downstream spacecraft		
$c = 10^{-3}$	All fits unsuccessful	All fits unsuccessful
$c = 10^{-4}$	1 close to successful fit	2 close to successful fits
$c = 10^{-5}$	All fits successful	All fits successful
Upstream spacecraft		
$c = 10^{-3}$	All fits unsuccessful	All fits unsuccessful
$c = 10^{-4}$	All fits successful	2 fits successful
$c = 10^{-5}$	All fits successful	All fits successful

Table 4. Comparison of the classical parameter fitted values to the "true" ones. Only outcomes following a converging fit, starting with the initial parameter values equal to the true ones, are presented in this table

Spacecraft	c	λ_r "True" (AU)	λ_r "Fitted" (AU)	λ_r σ(AU)	λ_r Ratio fit/true	λ_r Ratio true/fit	χ^2_v Flux	χ^2_v Anisotropy	χ^2_v Flux and anisotropy
Upstream	1.0E−04	0.0792	0.084	0.001	1.06	0.94	0.126	0.097	0.111
Upstream	1.0E−04	0.0792	0.080	0.001	1.01	0.99	0.309	0.105	0.205
Downstream	1.0E−04	0.0792	0.105	0.001	1.32	0.76	16.859	3.474	10.080
Downstream	1.0E−04	0.0792	0.101	0.001	1.27	0.79	18.309	4.525	11.321
Upstream	1.0E−04	0.277	0.371	0.010	1.34	0.75	0.216	0.051	0.132
Upstream	1.0E−04	0.277	0.560	0.015	2.02	0.50	0.260	0.195	0.226
Upstream	1.0E−04	0.277	0.309	0.005	1.11	0.90	0.351	0.197	0.272
Downstream	1.0E−04	0.277	0.809	0.007	2.92	0.34	10.786	6.443	8.542
		t_c "True" (h)	t_c "Fitted" (h)	t_c σ (h)	t_c Ratio fit/true	t_c Ratio true/fit			
Upstream	1.0E−04	1.500	0.794	0.034	0.53	1.89	0.126	0.097	0.111
Upstream	1.0E−04	1.500	1.315	0.029	0.88	1.14	0.309	0.105	0.205
Downstream	1.0E−04	1.500	0.258	0.008	0.17	5.80	16.859	3.474	10.080
Downstream	1.0E−04	1.500	0.383	0.023	0.26	3.91	18.309	4.525	11.321
Upstream	1.0E−04	1.500	0.870	0.041	0.58	1.72	0.216	0.051	0.132
Upstream	1.0E−04	0.500	0.716	0.066	1.43	0.70	0.260	0.195	0.226
Upstream	1.0E−04	1.500	0.870	0.025	0.58	1.72	0.351	0.197	0.272
Downstream	1.0E−04	0.500	0.875	0.024	1.75	0.57	10.786	6.443	8.542
		t_l "True" (h)	t_l "Fitted" (h)	t_l σ(h)	t_l Ratio fit/true	t_l Ratio true/fit			
Upstream	1.0E−04	0.500	0.954	0.054	1.91	0.52	0.126	0.097	0.111
Upstream	1.0E−04	2.000	2.345	0.061	1.17	0.85	0.309	0.105	0.205
Downstream	1.0E−04	2.000	36.997	5.420	18.50	0.05	16.859	3.474	10.080
Downstream	1.0E−04	0.500	0.319	0.025	0.64	1.57	18.309	4.525	11.321
Upstream	1.0E−04	0.500	0.599	0.034	1.20	0.84	0.216	0.051	0.132
Upstream	1.0E−04	0.100	0.066	0.007	0.66	1.51	0.260	0.195	0.226
Upstream	1.0E−04	2.000	2.949	0.099	1.47	0.68	0.351	0.197	0.272
Downstream	1.0E−04	0.100	0.068	0.002	0.68	1.47	10.786	6.443	8.542

Only fits that have been successful for both spacecraft and for the same set of searched parameters, are shown.

The difference between the true and fitted values of the classic parameters can be either negligible or very significant. The ratio between the fitted and true λ_r values is always higher than 1 and can be up to $\sim$3; i.e., λ_r can be overestimated by a factor $\sim$3. The values of t_c and t_l can be either overestimated or underestimated. The t_c parameter can be overestimated by a factor of up to $\sim$2 and underestimated by a factor of up to $\sim$6. The t_l parameter can be overestimated by a factor of up to $\sim$18 and underestimated by a factor of up to $\sim$2. Since these are only examples, the values of those maximum factors have to be understood as minimum ones.

For a given set of searched parameter values, the mean free path is always more overestimated at the downstream spacecraft. This is only due to the sign of the CFG. Negative intensity CFG would produce underestimated mean free path values. Therefore, depending on the sign of the CFG, the mean free path will be either over or underestimated. The value of the fitted mean free path can vary by up to at least 40% (true: $\lambda_r = 0.277$ AU, $t_c = 0.5$ h, $t_l = 0.1$ h) between the spacecraft, for this given configuration.

In conclusion, depending on the configuration of the spacecraft location and of the profile of the intensity CFG, if neglected, the influence of the latter on the classic parameter can vary from insignificant to very significant, the values being either under or overestimated.

3 Rules for multi-spacecraft analysis of associated independent physical processes

This section aims to determine some basic conditions that would make possible the identification of the type of CFG detected by multi-spacecraft analysis. When fitting data we want to find the best values of the parameters of the mathematical equation believed to describe the phenomenon (e.g., the flux profile). This is done by trying to minimise the χ^2 given in Eq. (14). For clarity, let us assume that there are only two parameters, p_0 and p_1, controlling the theoretical equation. In the best case, the values of χ^2 will form a surface, in the (χ^2, p_0, p_1) space, having one, and only one, minimum value. The position of that minimum will give the desired p_0 and p_1 values. However, the χ^2 surface might not have such well-defined unique minimum points. It might have either a multitude of minimum points or be trench-like in shape. In the first case the p_0 and p_1 values are well defined but show numerous roots. In the second case,

there is an infinity of roots; it is equivalent to an undetermined system of simultaneous equations, where the number of parameters is higher that the number of independent equations. Therefore, the first step is to find a way of having a finite number of roots and the second step is to try to identify which root is the correct one.

If we want to identify a finite number of roots when a trench is likely then we need to calculate another χ^2, derived from the comparison of a different phenomenon with another theoretical equation (e.g. the anisotropy profile). The key point is that all theoretical equations must use same p_0 and p_1 parameters that must have the same numerical values; called hereafter the identity condition. The overlapping of the two χ^2 surfaces may provide this finite number of roots since only the (p_0, p_1) values that give a minimum value for both χ^2 values are kept. However, unless one has a full knowledge of the χ^2 surfaces, this might not be enough since trenches of the χ^2 surfaces may share some common areas. Therefore, it is better to have the number of independent functions at least equal to, and preferentially higher than, the number of parameters. This is the equivalent to an over-constrained system of simultaneous equations and will later be referred to as the solvability condition. Two profiles are independent if their ratio evolves with changes in the values of the parameters used in the theoretical equations describing them.

There is no unique method to identify one root from others and not even an obvious way to know in advance whether there is more than one root possible. It is a problem similar to the one related to the trenches and the solvability condition applies: the more over-constrained the system, the higher are the chances of getting a good set of parameters. To increase the overestimation of the system one can increase the number of constraints or decrease the number of parameters.

Increasing the number of phenomena can be done by using several spacecraft. The potential new number is equal to the number of phenomena per spacecraft multiplied by the number of spacecraft. However, the independent condition must be satisfied to be applicable. For instance, it would not work if we want to identify potential ambiguities between the t_c and t_l parameters of Eq. (5) since, for those parameters, the SEP profiles are not spacecraft position-dependent. However, it would certainly work if we want to identify the CFG.

Decreasing the number of parameters is possible only if the parameters can be uniquely grouped, among the different equations, into well identified sub-equations. In that case, if an equation contains more than one parameter, several combinations of those parameters may lead to identical results of the sub-equation. We can then choose to search for the results of the sub-equation rather than for an accurate values of the parameters. For instance, the empirical equation used to describe the cross-field gradients contains four parameters. However, at this level of the study, what matters is more the profile of the CFG than the numerical values of those parameters. That is why, in the latter, the CFG profile will be considered as only one "parameter".

So far only three independent phenomena, for which theoretical functions have been established, have been identified and used to analyse the SEP profiles: (a) the flux intensity, (b) the anisotropy, (c) the pitch angle distributions (PADs). The flux intensity and anisotropy profiles are used to find the values of the mean free path and the finite injection profile $I(t)$ (see Eq. 5). Indeed, if only the flux was used then there would be a trench between the mean free path on one side and the $I(t)$ profile on the other side. It has to be noted that $I(t)$ has two parameters, called t_c and t_l, that need to be fitted. This, a priori, violates the solvability condition unless we assume that there is no ambiguity in the two parameters value or consider $I(t)$ as a single parameter. Assuming that there is no ambiguity means that, having fixed the mean free path, it is assumed that there is no trench in the χ^2 surface generated by the (t_c, t_l) parameters. The third piece of information, provided by the PADs, is used to characterise the variation of the mean free path with the distance (assuming that $\kappa(z, \mu) = \kappa(z) \times \kappa(\mu)$ as shown in Kunow *et al.*, 1991) and the finite injection profile. All of this is valid if it is assumed that any other features influencing the SEP profiles are neglected, i.e. considered as "difficulties" (Kunow *et al.*, 1991).

Therefore, this section demonstrates, that multi-spacecraft analysis can be used to differentiate among the various type of CFG if, across the phenomena and the spacecraft, the identity, independence and solvability conditions are fulfilled.

4 Conclusion

The general concept of CFG has been presented. It is a generic name designating spatial variations, in the solar wind frame, of the physical quantities controlling the shape and amplitude of the SEP profiles. The particular case of intensity CFG has been discussed and its influence on the estimation of the classic parameters (i.e. λ_r, t_c and t_l) assessed.

It has been shown that a CFG as simple as the one originating in spatial variations of the source intensity can influence significantly the shape of the flux profile. If intensity CFGs, as such, exist, then two spacecraft, located at 1 AU from the Sun and separated radially by 10^6 km ($\Phi = 0.3°$), are well positioned to identify reductions of the intensity of the injection of two orders of magnitude over distances of $\sim 10^4$ km ($\Phi = \sim 1°$) at the solar surface.

It has also been shown that, if CFG are neglected, then the numerical values of the classic parameters can be under or overestimated by factors that can reach at least $\sim$2–3 for the parallel mean free path (λ_r). They can also be under or overestimated by a factor up to at least $\sim$6 and $\sim$18 for, respectively, the t_c and t_l parameters.

Three basic requirements needed to identify the origin of the CFG from multi-spacecraft analysis have been proposed. They have been called (a) the solvability, (b) independence and (c) identity conditions. The (a) solvability condition states that the number of param-

eters (or profiles) that can be assessed should be lower or equal to the number of independent profiles that can be fitted. The (b) independence condition states that two profiles are independent if their ratio evolves with changes in the values of the parameters. The (c) identity condition states that the parameters to be fitted must represent the same quantities and have the same numerical values across all the spacecraft and phenomena used.

The spacecraft linked to the International Solar Terrestrial Physics (ISTP) project are particularly well suited and well positioned to study CFGs. The fleet of ISTP (or associated) spacecraft is very likely to fulfil the identity condition. Indeed most of them, because they are all in the Earth's vicinity, are likely to be considered as being crossed by the same field lines (all depending on the solar wind velocity) and in a time frame valid for studying SEP. Unfortunately, most of them orbit around the Earth. This means that they are not in the solar wind the whole time i.e. a multi-spacecraft analysis of one particular event will depend on how many spacecraft are in the solar wind at the time of the event.

Acknowledgements. I am very grateful to Dr. E. Roelof for his valuable scientific comments and his help for getting the paper into shape. I am also very grateful to Dr. Mike Hapgood for his support and recommendations thoughout the preparation of this work. Finally, I thank Pr. R. P. Lin and Dr. L. J. Lanzerotti for their, always relevant, comments.

Topical Editor R. Schwenn thanks M. B. Kallenrode and E. C. Roelof for their help in evaluating this paper.

Appendix: estimation of the flux and anisotropy uncertainties

Information from particle detectors comes from counts measured in individual angular sectors. These counts are then transformed into various units depending on the scientific purpose. The uncertainty on the number of counts is usually assumed to follow Poisson's law and therefore to be equal to:

$$\sigma_l^c = \sqrt{y_l^c}$$

where c, means *counts*, and l the sector number. However, the values fitted here are expressed in differentiated flux units ($1/\mathrm{cm}^2.\mathrm{sr.s.keV}$). Therefore:

$$y_l^f = \alpha^2 y_l^c$$

with "f", meaning "flux". Since:

$$\frac{\sigma_l^f}{y_l^f} = \frac{\sigma_l^c}{y_l^c}$$

then

$$\sigma_l^f = \alpha^f \sqrt{y_l^f} \ .$$

Estimation of σ^f

This expression is valid for measurements made in individual sectors and the uncertainty for omnidirectional flux must be derived from it. The net flux is calculated from the flux in each PAD as followed:

$$y^f = \frac{1}{4\pi}\sum_{l=0}^{L} y_l^f \Delta\Omega_l$$

where $\Delta\Omega_l$ is the solid angle swept by a given sector or pitch angle of index l. Therefore:

$$\sigma^f = \frac{1}{4\pi}\sum_{l=0}^{L} \sigma_l^f \Delta\Omega_l$$

$$\sigma^f = \frac{\alpha^f}{4\pi}\sum_{l=0}^{L} \sqrt{y_l^f}\,\Delta\Omega_l$$

If the flux is isotropic then we get back:

$$\sigma^f = \alpha^f \sqrt{y^f}$$

Indeed:

$$y^f = \frac{1}{4\pi}\sum_{l=0}^{L} y_l^f \Delta\Omega_l$$

$$y^f = y_l^f \frac{1}{4\pi}\sum_{l=0}^{L} \Delta\Omega_l$$

$$y^f = y_l^f$$

Therefore:

$$\alpha^f \sqrt{y_l^f} = \text{const.} = \alpha^f \sqrt{y^f}$$

$$\sigma^f = \alpha^f \sqrt{y^f} \frac{1}{4\pi}\sum_{l=0}^{L} \Delta\Omega_l$$

$$\sigma^f = \alpha^f \sqrt{y^f}$$

which is the expression to be used.

Estimation of σ^a

The anisotropy for both the model and the data has been calculated using the expression (from, e.g., Kunow, 1991):

$$\xi = \frac{\sum_{l=0}^{L} \mu_l y_l^f \Delta\Omega_l}{\sum_{l=0}^{L} y_l^f \Delta\Omega_l}$$

μ being the cosine of the pitch angle. The value of ξ is equal to 0 and 1 if the flux is, respectively, symmetric with respect to the 90° pitch angle and field aligned along one direction (ξ has to be understood as equal to $|\xi|$).
Therefore:

$$\sigma^a = \xi\left(\frac{\sum_{l=0}^{L} \sigma_l^f \Delta\Omega_l}{\sum_{l=0}^{L} y_l^f \Delta\Omega_l} + \frac{\sum_{l=0}^{L} |\mu_l \Delta\Omega_l \sigma_l^f|}{\sum_{l=0}^{L} |\mu_l \Delta\Omega_l y_l^f|}\right)$$

$$\sigma^a = \xi\left(\frac{\frac{\alpha^f}{4\pi}\sum_{l=0}^{L} \sqrt{y_l^f}\,\Delta\Omega_l}{y^f} + \frac{\sum_{l=0}^{L} |\mu_l \Delta\Omega_l \alpha^f \sqrt{y_l^f}|}{\sum_{l=0}^{L} |\mu_l \Delta\Omega_l y_l^f|}\right)$$

For an isotropic flux we get:

$$\sigma^a = 2\xi \frac{\alpha^f}{\sqrt{y^f}} \ .$$

Although the flux intensity stays high, the anisotropy quickly drops to values close to zero. Therefore, the points carrying the information are concentrated around the onset and therefore limited in number. Most of the anisotropy values are low and,

when measured, quite statistical. Hence, if their associated uncertainties are too small then those points will be the main contributor to the value of the χ_v^2. Their statistical distribution will be the main driver of the fit instead of the smallest one (they usually lead to a flattening of the fitted anisotropy profile). Increasing α^f will not help because it will also increase the uncertainty of high anisotropy values. What is required is an expression that increases faster (than this one) the relative uncertainties with the decrease of ξ_n. That is why it has been arbitrarily chosen to use:

$$\sigma^a = \frac{\alpha^a}{\sqrt{y^f}}$$

Validity of the "isotropic" approximation

Mathematically speaking, the "isotropic" approximation gives maximum values of σ_n^f and therefore a minimum χ_v^2 value. Indeed, let us assume the extreme case where the flux is highly anisotropic and concentrated in one pitch angle, then:

$$y^f = \frac{1}{4\pi} y_l^f \Delta\Omega_l$$

$$y_l^f = \frac{4\pi y^f}{\Delta\Omega_l}$$

$$\sigma^f = \alpha^f \sqrt{y_l^f} \frac{\Delta\Omega_l}{4\pi}$$

$$\sigma^f = \alpha^f \sqrt{y^f} \sqrt{\frac{\Delta\Omega_l}{4\pi}}$$

Since:

$$\sqrt{\frac{\Delta\Omega_l}{4\pi}} < 1$$

the "isotropic" σ^f is therefore larger than the "anisotropic" one. This would be similar for the uncertainty of the anisotropy.

References

Anderson, K. A., and W. M. Dougherty, A spatially confined long-lived stream of solar particles, *Solar Phys.*, **103,** 165–175, 1986.

Anderson, K. A., P. A. Chaizy, R. P. Lin, and J. Sommers, Non-relativistic solar electron events during December 1990: results from Ulysses, *Geophys. Res. Let.*, **19,** (12), 1283–1286, 1992.

Anderson, K. A., J. Sommers, R. P. Lin, M. Pick, P. A. Chaizy, N. Murphy, E. J. Smith, and J. L. Phillips, Mirroring of fast solar flare electrons on a downstream corotating interaction region, *J. Geophys. Res.*, **100,** (A1), 3–11, 1995.

Axford, W. I., Anisotropic diffusion of solar cosmic rays, *Planet. Space Sci.*, **13,** 1301–1309, 1965.

Bevington, P. R., and D. K. Robinson, *Data reduction and error analysis for the physical sciences*, McGraw-Hill, 1994.

Bieber, J. W., W. H. Matthaeus, C. W. Smith, W. Wanner, M.-B. Kallenrode, and G. Wibberenz, Proton and electron mean free paths: the Palmer consensus revisited, *Astrophys. J.*, **420,** 294–306, 1994.

Hasselmann, K., and G. Wibberenz, Scattering of charged particles by random electromagnetic fields, *Z. Geophys.*, **34,** 353–388, 1968.

Jokipii, J. R., Cosmic ray propagation. I charged particles in a random magnetic field, *Astrophys. J.*, **146,** 480–487, 1966.

Kallenrode, M.-B., Particle propagation in the inner heliosphere, *J. Geophys. Res.*, **98,** (A11), 19,037–19,047, 1993.

Kallenrode, M.-B., and G. Wibberenz, Propagation of particles injected from interplanetary shocks: a black box model and its consequences for acceleration theory and data interpretation, *J. Geophys. Res.*, **102,** (A10), 22,311–22,334, 1997.

Kunow, H., G. Wibberenz, G. Green, R. Muller-Mellin, and M.-B. Kallenrode, Energetic particles in the inner solar systems, Physics of the Inner Heliosphere II, Eds. R. Schwenn, and E. Marsch, Springer, Berlin Heidelberg New York, 243–342, 1991.

Lario, D., B. Sanahuja, and A. M. Heras, Energetic particle events: efficiency of interplanetary shocks as $50\,\mathrm{keV} < E < 100$ MeV proton accelerators, *Astrophys. J.*, **509,** 415–434, 1998.

Lin, R. P., Non-relativistic solar electrons, *Space Sci. Rev.*, **16,** 189–256, 1974.

Lin, R. P., and S. W. Kahler, Interplanetary magnetic field connection to the Sun during electron Heat flux dropouts in the solar wind, *J. Geophys. Res.*, **97,** (A6), 8203–8209, 1992.

Lin, R. P., K. A. Anderson, S. Ashford, C. Carlson, D. Curtis, R. Ergun, D. Larson, J. McFadden, M. McCarthy, G. K. Parks, H. Reme, J. M. Bosqued, J. Coutelier, F. Cotin, C. d'Uston, K.-P. Wenzel, T. R. Sanderson, J. Henrion, J. C. Ronnet, and G. Paschmann, A three-dimensional plasma and energetic particle investigation for the WIND spacecraft, *Space Sci. Rev.*, **71,** (1–4), 123–153, 1995.

Maia, D., M. Pick, A. Kerdraon, R. Howard, G. E. Bruckner, D. J. Michels, S. Paswaters, R. Schwenn, P. Lamy, A. Llebaria, G. Simnett, and H. Aurass, Joint Nancay radioheliograph and Lasco observations of coronal mass ejections I- the July 1, 1996 event, *Solar Phys.*, (in press), 1998.

Morfill, G., A. K. Richter, and M. Scholer, Average properties of cosmic ray diffusion in solar wind streams, *J. Geophys. Res.*, **84,** (A4), 1505–1513, 1979.

Ng, C. K., and L. J. Gleeson, A complete model of the propagation of solar-flare cosmic rays, *Solar Phys.*, **46,** 347–375, 1976.

Ng, C. K., and K.-Y. Wong, Solar particle propagation under the influence of pitch-angle diffusion and collimation in the interplanetary magnetic field, *Proc. Int. Conf. Cosmic Rays* 16th, **5,** 252–257, 1979.

Numerical Recipes, Cambridge, Cambridge University Press, 1989.

Palmer, I. D., Transport coefficients of low-energy cosmic rays in interplanetary space, *Rev. Geophys. Space Phys.*, **20,** (2), 335–351, 1982.

Parker, E. N., The passage of energetic charged particles through interplanetary space, *Planet. Space Sci.*, **13,** 9–49, 1965.

Pick, M., D. Maia, A. Kerdraon, R. Howard, G. E. Bruckner, D. J. Michels, S. Paswaters, R. Schwenn, P. Lamy, A. Llebaria, G. Simnett, and H. Aurass, Joint Nancay radioheliograph and Lasco observations of coronal mass ejections II- the July 9, 1996 event, *Solar Phys.*, (in press), 1998.

Reid, G. C., A diffusive model for the initial phase of a solar proton event, *J. Geophys. Res.*, **69,** (13), 2659–2667, 1964.

Roelof, E. C., Propagation of solar cosmic rays in the interplanetary magnetic field, in *Lectures in High Energy Astrophysics*, 111–135, Eds. H. Ogelman and J.R. Wayland (NASA SP-199), 1969.

Scholer, M., G. Morfill, and A. K. Richter, Energetic solar particle events in a stream-structured solar wind, *Solar Phys.*, **64,** 391–401, 1979.

Schulze, B. M., A. K. Richter, and G. Wibberenz, Influence of finite injections and of interplanetary propagation on time-intensity and time-anisotropy profiles of solar cosmic rays, *Solar Phys.*, **54,** 207–228, 1977.

Wanner, W., and G. Wibberenz, A study of the propagation of solar energetic protons in the inner heliosphere, *J. Geophys. Res.*, **98,** (A3), 3513–3528, 1993.

Wibberenz, G., K. Hasselmann, and D. Hasselmann, Comparison of particle-field interaction theory with solar proton diffusion coefficients, *Acta Phys. Acad. Sci. Hung.*, Suppl., **29**(2), 37, 1970.

Wibberenz, G., K. Kecskemety, H. Kunow, A. Somogyi, B. Iwers, Y.-I. Logachev, and V. G. Stolpovskii, Coronal and interplanetary transport of solar energetic protons and electrons, *Solar Phys.*, **124,** 353–392, 1989.